We are IntechOpen, the world's leading publisher of Open Access books Built by scientists, for scientists

6,900
Open access books available

186,000
International authors and editors

200M
Downloads

154
Countries delivered to

Our authors are among the
TOP 1%
most cited scientists

12.2%
Contributors from top 500 universities

BOOK CITATION INDEX
CLARIVATE ANALYTICS
INDEXED

WEB OF SCIENCE™

Selection of our books indexed in the Book Citation Index
in Web of Science™ Core Collection (BKCI)

Interested in publishing with us?
Contact book.department@intechopen.com

Numbers displayed above are based on latest data collected.
For more information visit www.intechopen.com

Mode Interferences of VLF Waves in the Presence of an Anisotropic Terrestrial Waveguide

Ting Ting Gu and Hong Lei Xu

Abstract

It is known that the very low frequency (VLF) signals propagating at long distances over a terrestrial waveguide will experience a diurnal interference across the sunrise and sunset transitions. Early studies indicated that cascaded terrestrial waveguides can be applied to investigate the cycle-clip behaviors of amplitude and phase for VLF waves, with an abrupt effective height change by 20 km to represent the night and day transitions. Based on the knowledge, this chapter starts with some basic concepts on VLF wave propagation in the presence of an anisotropic terrestrial waveguide. Then, by performing the method of field matching at the discontinuous junctions, the coefficients of transmitted and scattered vectors are resulted from two derived matrix equations. Finally, the synthetic fields are calculated to simulate the VLF waves, which are subjected to an oblique geomagnetic field during long-distance propagation. The purpose of the present chapter is to illustrate the disturbing nature during sunrise and sunset for the VLF waves with periodic variations in amplitudes interfered by multimodes over long propagation paths.

Keywords: VLF waves, mode-conversion coefficient, sunrise transition, sunset transition, terrestrial cascaded waveguides

1. Introduction

The very low frequency (VLF) waves, namely, the radio waves whose wavelengths are between 10 and 100 km and operate at the frequencies ranging from 3 to 30 kHz, are usually used for long-distance propagations. In this frequency band, both the ground medium (occupied by land, lake, or seawater) and the ionosphere (the sky region of the height over 60–90 km distinct from daytime to nighttime states) are strongly reflecting for the excited waves, so that the VLF waves are conducted to propagate in free space between the two parallel reflecting walls. This is the so-called terrestrial waveguide. Generally, a vertical electric dipole antenna, polarized in perpendicular to the ground interface, can be idealized to generate these guiding waves in transverse magnetic (TM) modes, whereas the transverse electric (TE) modes generated by a horizontally polarized electric dipole antenna would not propagate along the radial direction. Assuming that the spherical coordinate system has been established, "the ground-ionosphere waveguide" is formed by the two concentric spherical shells.

Along a great propagation path across two states of the daytime and nighttime sections, the resulted cycle clips by interferences would be observed in phase for VLF radio waves [1–7]. Most of the early explanations of this phenomenon [8–10] were based on the ray-optic model; however, it seems unlikely to be accountable correctly for the mentioned matter for a long-distance propagation. That is because, on the one hand, it would be required to include lots of ray paths in explaining the VLF wave propagation at great distances, yet only a few low-order modes are necessary; and on the other hand, there should be consideration of including the diffraction corrections for using ray-optic models over a curved earth.

For a better knowledge of diurnal behaviors as phase and amplitude variations for VLF radio waves, extensive studies had been developed over the years by researchers. In the 1960s, the effect of multimode interferences had been addressed by Wait [11, 12] for VLF radio waves in the presence of a nonuniform earth-ionosphere waveguide. Later, the study had been extended by Bahar in the 1970s [13–16] where the inhomogeneous waveguide was assumed to be represented by successive cascaded earth-ionosphere waveguides, for which the height variations were accounted for the day-to-night transition. In these analyses, the mode-conversion coefficients had been formulated by employing the orthogonal properties of basis functions. Consequently, the resulted coefficients could be utilized to derive a set of coupled first-order differential equations for the forward and backward wave amplitudes in the transition region, to extend the study into a more general case with arbitrarily varying effective height. However, it should be pointed out that these computational schemes by previous treatments had neglected the influence of the geomagnetic field. In the study by Galejs [17, 18], the transition geometry of waveguide with an abrupt height change of dh was equivalent to that of a waveguide with identical height boundaries but different surface impedances, representing the anisotropic ionosphere in daytime and nighttime, respectively. However, the author also indicated the derived reflection coefficients would be of even smaller significance in a more realistic problem of gradual height or impedance changes. Therefore, the mode-conversion coefficients remain to be formulated for higher accuracy of the VLF radio waves to include the influence of geomagnetic field at great propagation path across daytime and nighttime states.

The analytical formulas for mode-conversion coefficients have been derived in the circadian transitional period by Pan et al. [19–21] applied in ELF/SLF electromagnetic wave propagation in earth-ionosphere waveguide due to sunrise and sunset. Apart from its simplicity, the proposed computations are also feasible for studying the influence of the anisotropic behavior from the ionosphere, including reflection characteristics of the transitional daytime and nighttime sections. The study leads us to treat the ionosphere as anisotropic plasma medium and derive the mode-conversion coefficients resulted from the daytime and nighttime transitions for VLF waves.

In this chapter, the matter of VLF wave propagation is addressed in the presence of an earth-ionosphere cavity. Considering the diurnal behavior caused by sunrise and sunset transitions, the mode-conversion coefficients in an earth-ionosphere waveguide have been derived under an abrupt effective height change. The proposed computational scheme guarantees satisfactory accuracy of the electromagnetic field in the transition ranges and can be developed in the derivation of the coupled differential equations for the wave amplitudes in a transition section of gradually varying height. Additionally, the mode interference has been analyzed. The time dependence $e^{i\omega t}$ is suppressed throughout the analysis.

2. VLF radio wave propagation in the presence of an anisotropic earth-ionosphere waveguide

In this section, the expressions of electromagnetic components have been addressed for VLF radio waves propagating in an anisotropic earth-ionosphere waveguide. The computations are based on an analysis of exploiting the concept that the VLF radio waves propagate in a spherical earth-ionosphere waveguide, with finite surface impedance boundaries. Wave components are formulated in the expression of Airy functions for the VLF radio waves in the context.

2.1 Formulation

Assume that the strength of geomagnetic field B_0 is suppressed by an oblique incident angle θ_0 in $\hat{z}$ direction (the direction perpendicular to the interface of the earth) in the $\hat{x}$-$\hat{z}$ plane. The ionosphere above the air is regarded as the homogeneous anisotropic plasma, characterized by a tensor permittivity $\acute{\varepsilon}$ [22], which is defined by

$$\acute{\varepsilon}_{A,B} = \varepsilon_0(I + M_{A,B}) \tag{1}$$

in which the constant ε_0 represents for the free-space permittivity, I is a 3×3 unit matrix, and the susceptibility of ionosphere M can be expressed as follows:

$$M = \frac{-X}{U(U^2 - y^2)} \\ \times \begin{bmatrix} U^2 - l^2 y^2 & inUy & -ln\,y^2 \\ -inUy & U^2 & ilUy \\ -ln\,y^2 & -ilUy & U^2 - n^2 y^2 \end{bmatrix} \tag{2}$$

where the variable U is the effective electron collision frequency of the ionosphere, defined by $U = 1 + i\nu/\omega$, $y = \omega_H$, and $X = \omega_0^2/\omega^2$; ω_H and ω_0 are the gyrofrequency of the electrons and angular plasma frequency of the ionosphere, respectively; and l and n are the directional cosines of the geomagnetic field in the $\hat{x}$ and $\hat{z}$ directions, respectively.

2.2 Expressions of the components for VLF radio waves in an anisotropic terrestrial waveguide

In what follows, it is assumed that the characteristics of VLF radio waves are determined by propagation paths from the exciting source to the receiving field point, that is, the characteristics of propagation will not be affected by other propagation paths.

2.2.1 Computational expressions

In an idealized geometry, the ionosphere layers are regarded as the anisotropic plasma, and the waveguide is occupied by free space, characterized by the permeability μ_0 and uniform permittivity ε_0. The spherical earth is characterized by the permeability μ_0, uniform permittivity ε_g, and conductivity σ_g. Considering the anisotropic properties of the ionosphere, the wave components for VLF radio waves

in the earth-ionosphere waveguide would be no longer strictly separated by TM waves and TE waves [23, 24]. Each wave type will consist of six electromagnetic wave components expressed in the following form:

$$
\begin{matrix} E_{rn} \\ E_{\theta n} \\ E_{\phi n} \\ H_{rn} \\ H_{\theta n} \\ H_{\phi n} \end{matrix} = a_n \begin{Bmatrix} F_n(t_n, y) \\ i\beta_n^{-1} F_n'(t_n, y)/k \\ \Delta_{Emn} g_n(t_n, y)\beta_n^{-1} \\ \Delta_{Emn} g_n(t_n, y) \\ i\Delta_{Emn} g_n'(t_n, y)\beta_n^{-1}/k \\ -\beta_n^{-1} F_n(t_n, y) \end{Bmatrix} e^{ika\beta_n\theta} \tag{3}
$$

in which the functions $F_n(z)$ and $g_n(z)$ stand for the normalized "height-gain" functions for the TE mode and TM mode, respectively, defined by

$$
F_n(y) = \frac{w_2(t_n - y) + B_1(t_n)w_1(t_n - y)}{w_2(t_n) + B_1(t_n)w_1(t_n)} \tag{4}
$$

$$
g_n(y) = \frac{w_2(t_n - y) + B_2(t_n)w_1(t_n - y)}{w_2(t_n) + B_1(t_n)w_1(t_n)} \tag{5}
$$

in which

$$
B_1(t_n) = \frac{-w_2'(t_n) - qw_2(t_n)}{w_1'(t_n) - qw_1(t_n)}; \quad B_2(t_n) = \frac{-w_2'(t_n) - q^h w_2(t_n)}{w_1'(t_n) - q^h w_1(t_n)} \tag{6}
$$

with

$$
q = i\left(\frac{ka}{2}\right)^{\frac{1}{3}}\Delta_g; q^h = i\left(\frac{ka}{2}\right)^{\frac{1}{3}}\frac{1}{\Delta_g} \tag{7}
$$

In the above formulas, the variable β_n is the nth wave impedance defined by $\beta_n = 1 + t_n[2/(ka)]^{2/3}/2$, and the sequential roots t_n are determined by the modal equation in [5], rewritten as follows:

$$
\begin{aligned}
&\left[w_2'(t_n - y_0) + i\Delta_{11}\left(\frac{ka}{2}\right)^{\frac{1}{3}}w_2(t_n - y_0) \right.\\
&\left. + B_1(t_n)\left(w_1'(t_n - y_0) + i\Delta_{11}\left(\frac{ka}{2}\right)^{\frac{1}{3}}w_1(t_n - y_0) \right) \right]\\
&\times \left\{ \Delta_{22}w_2'(t_n - y_0) - i\left(\tfrac{ka}{2}\right)^{\frac{1}{3}}w_2(t_n - y_0) \right.\\
&\left. + B_2(t_n)\left[\Delta_{22}w_1'(t_n - y_0) - i\left(\tfrac{ka}{2}\right)^{\frac{1}{3}}w_1(t_n - y_0) \right] \right\}\\
&- i\left(\tfrac{ka}{2}\right)^{\frac{1}{3}}\Delta_{12}\Delta_{21}\left[w_2'(t_n - y_0) + B_2(t_n)w_1'(t_n - y_0) \right]\\
&\times \left[w_2(t_n - y_0) + B_1(t_n)w_1(t_n - y_0) \right] = 0
\end{aligned} \tag{8}
$$

The coupling impedance Δ_{Emn} is expressed as

$$\Delta_{Emn} = M_n$$

$$\left\{ i\Delta_{21} \left(\frac{ka}{2}\right)^{\frac{1}{3}} \left[w_2(t_n - y_0) + B_1(t_n)w_1(t_n - y_0) \right] \right\}$$

$$\times \left\{ \Delta_{22}w_2'(t_n - y_0) - i\left(\tfrac{ka}{2}\right)^{\frac{1}{3}} w_2(t_n - y_0) \right. \tag{9}$$

$$\left. + B_2(t_n)\left[\Delta_{22}w_1'(t_n - y_0) - i\left(\tfrac{ka}{2}\right)^{\frac{1}{3}} w_1(t_n - y_0) \right] \right\}^{-1}$$

and the nth-mode wave admittance u is

$$Y_n = \beta_n / kZ_0 \tag{10}$$

where the variable Z_0 stands for the free-space wave impedance.

2.2.2 Definition of the airy functions

In the evaluation of Eq. (8) to Eq. (9), the Airy functions have been employed. In order to clarify these special functions, the following expressions provided by the use of Bessel functions are defined as follows [23]:

$$w_1(x) = e^{-i\frac{2\pi}{3}} \left(\frac{-\pi t}{3}\right)^{\frac{1}{2}} H_{1/3}^{(2)}\left[\frac{2}{3}(-t)^{\frac{3}{2}}\right] \tag{11}$$

$$w_2(x) = e^{+i\frac{2\pi}{3}} \left(\frac{-\pi t}{3}\right)^{\frac{1}{2}} H_{1/3}^{(1)}\left[\frac{2}{3}(-t)^{\frac{3}{2}}\right] \tag{12}$$

$$w_1'(x) = e^{-i\frac{\pi}{3}} \left(\frac{\pi}{3}\right)^{\frac{1}{2}} (-t) H_{2/3}^{(2)}\left[\frac{2}{3}(-t)^{\frac{3}{2}}\right] \tag{13}$$

$$w_2'(x) = e^{+i\frac{\pi}{3}} \left(\frac{\pi}{3}\right)^{\frac{1}{2}} (-t) H_{2/3}^{(1)}\left[\frac{2}{3}(-t)^{\frac{3}{2}}\right] \tag{14}$$

in which the Airy functions are defined by the first- and second-kind Hankel functions of one third or two third order. In addition, the Wronskian equality for the Airy function is defined as follows:

$$W = w_1 w_2' - w_2 w_1' = constant. \tag{15}$$

2.3 Computation and discussion

In what follows, the propagation parameters are computed for VLF waves and quantitatively compared to the isotropic case to study the anisotropic ionosphere properties influenced by the geomagnetic fields.

2.3.1 Impedance matrix of ionosphere

To consider an anisotropic ground-ionosphere waveguide, the surface imped- ance matrix for the field components has been applied to terminate the source-free
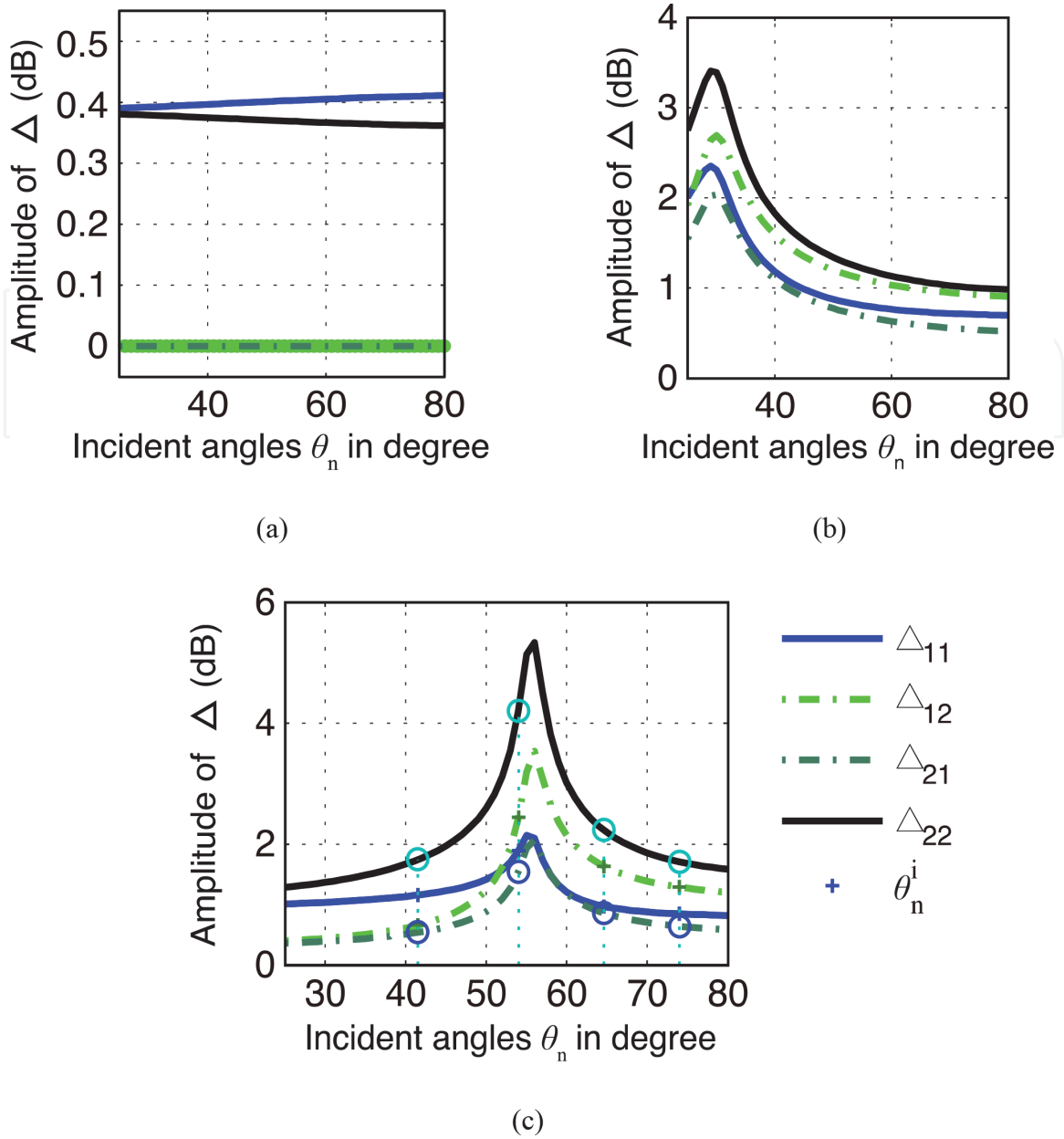
Figure 1.
The amplitudes of elements of the ionospheric impedance matrix versus the propagation direction θ_n, at f = 10 kHz, with strength of earth geomagnetic field: (a) 10^{-6} *G, (b)* 0.45 *G, (c)* 0.5 *G, respectively.*

waveguide at the same altitude as in the region of the waveguide source. In **Figures 1** and **2**, the elements of impedance matrix have been computed at an operating frequency by $f = 10kHz$ for anisotropic ionosphere, where the equivalent effective height of the ionosphere is assumed to be $h = 90km$ for summer daytime, electron density is N = 10^9 m^{-3}, and electron collision frequency is $\nu = 10^7$ s^{-1}. And the ground (assumed to be occupied by seawater) is characterized by the relative dielectric constant $\varepsilon_r = 80$ and the conductivity $\sigma = 5$ Sm^{-1}. In the numerical examples, the incident angles θ_n are selected, ranging from 10 to 80°, while the strength of earth geomagnetic field B_0 is chosen by 10^{-6} G, 0.45 G, and 0.5 G, respectively, where the inclination angle is characterized by a dip angle with $\vartheta = 0$, in east-to-south direction.

The diagonal elements Δ_{11} and Δ_{22} in the matrix of ionosphere surface impedance are accounted for the TM mode and TE mode, respectively, and the elements of ionosphere impedance matrix are affected by the earth geomagnetic field. Specifically, the curves of TM mode and TE mode are interfered more as suppressed by stronger earth geomagnetic field strengths.
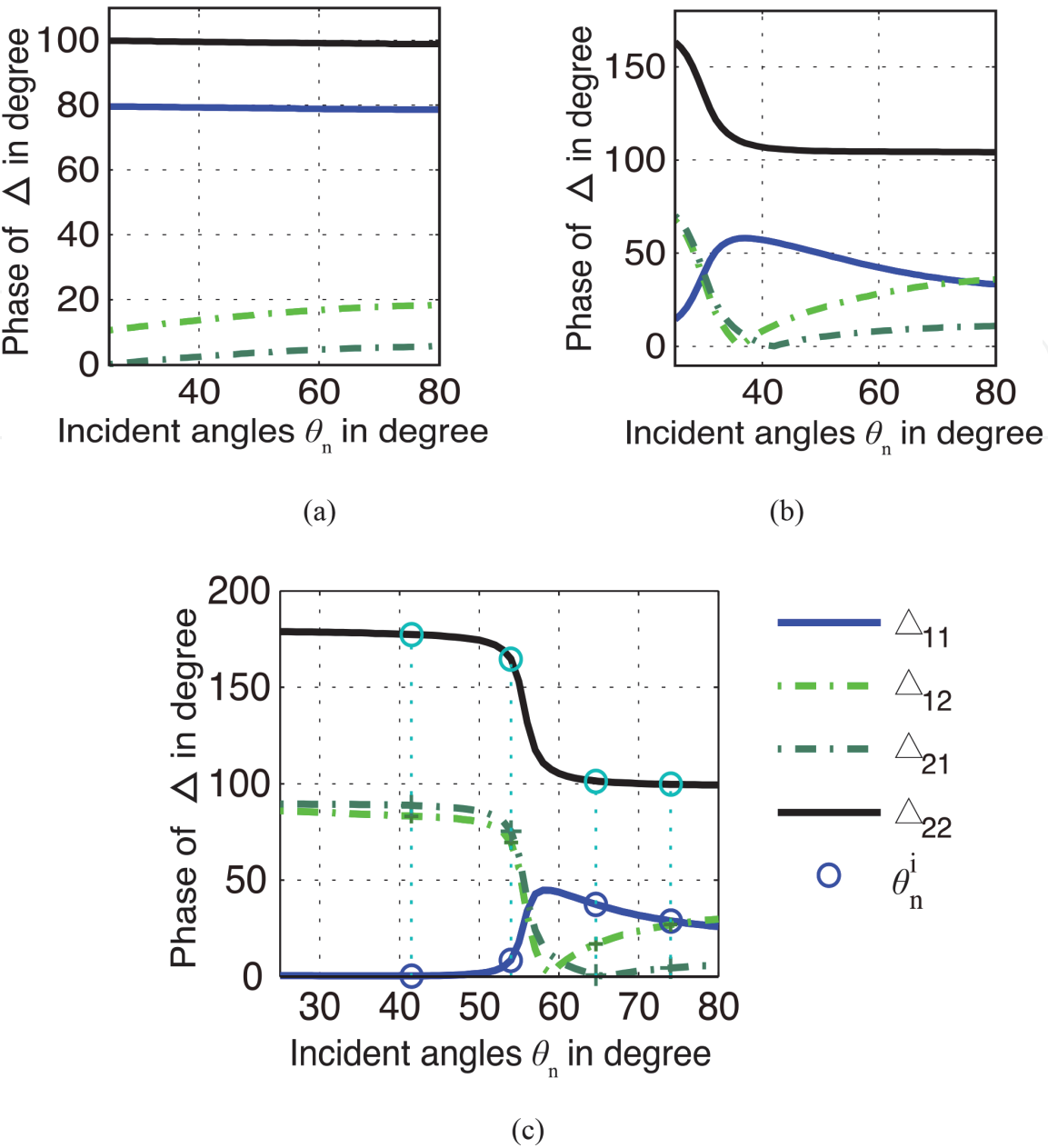
(a)

(b)

(c)

Figure 2.
The phases of elements of the ionospheric impedance matrix versus the propagation direction θ_n, at f = 10 kHz, with strength of earth geomagnetic field: (a) 10^{-6} G, (b) 0.45 G, (c) 0.5 G, respectively.

2.3.2 Attenuations and velocities of the VLF radio waves

At VLF radio frequencies, the surface impedance of the ground is much smaller than that of the ionosphere. This makes the change of the ground conductivity to have little effect on the phase velocity and attenuation rate of the waves [19]. In the following computations, the ground is assumed to be idealized to the sea surface. By the proposed formulas, we will compute the anisotropic ionosphere parameters. To begin with, the modal equation of VLF wave propagation can be solved readily by (8), so that the characteristic parameters are calculated correspondingly. In **Figures 3(a)** and **3(b)**, with the conductivity and the relative dielectric constant of sea water being $\sigma_g = 4$ S/m and $\varepsilon_{rg} = 80$, respectively, the attenuation rates α (dB/1000 km) are calculated with respect to the normalized frequencies (with $f_c = 10kHz$) where the boundary of the lower ionosphere is assumed at an altitude $h = 70$ km and $h = 90$ km for daytime and nighttime, respectively.

As is depicted from **Figure 3(a)**, the attenuation rates of lower modes are raised by increasing the operating frequencies. But for the higher modes, the attenuation
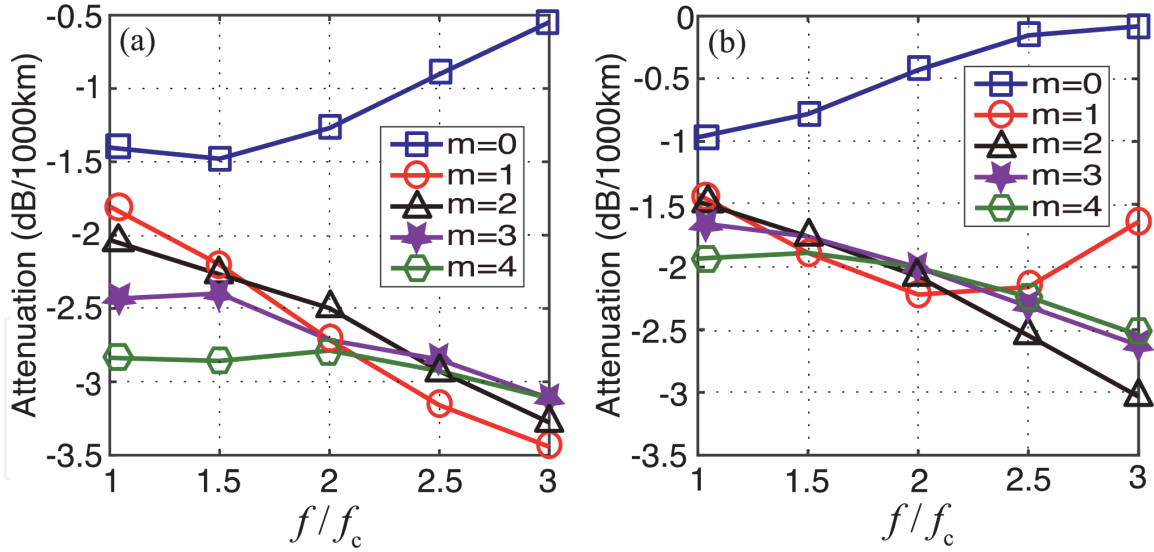
Figure 3.
The attenuation rates versus the normalized frequency f/f_c with (a) $h = 70km$ and (b) $h = 90km$, respectively.

rates decrease on the same condition. This is because the fundamental mode as the ground wave term cannot propagate at great propagation distances, whereas the high modes as sky waves, multi-reflected by the ground and ionosphere walls, will propagate through long path. Considering that both the radiating antenna and the receiving antenna are located in the same state of daytime or nighttime, the equivalent altitude of the ionosphere is quite different from each state along with propagation path. In **Figure 3**, it is shown that the attenuation rates of lower modes have different behaviors for daytime and nighttime [$m = 0$ in **Figure 3(a)** for daytime and $m = 0, 1$ in **Figure 3(b)** for nighttime], respectively, than the other modes as increased by operating frequency. Generally, it is seen that the higher effective ionosphere height is, the lower modes appear with attenuation rates as increased by frequencies.

As is shown in **Figures 4(a)** and **4(b)**, the relative phase velocities are evaluated, correspondingly, in variance of the normalized frequencies (with $f_c = 10kHz$) for daytime and nighttime, suppressed by earth geomagnetic field with the strength chosen as 0.45 and 0.5 Gauss, respectively. The formulas for VLF wave components in the presence of earth-ionosphere waveguide have been given in [12], as well as their special dispersive features by the propagation coefficients. It is noted that the relative velocities of VLF radio waves decrease as increased by operating frequencies. However, it is also known from **Figures 4(a)** and **(b)** that the phase velocity of the fundamental mode, standing for the ground wave, is affected very little by earth geomagnetic inclination angles, while that of the high modes changes greatly by the angles. Specifically, the influence of the relative phase velocity resulted from the earth geomagnetic field is about in the range of 1–3% [19].

In conclusion, the attenuation rates and phase velocities of the ground wave mode are affected by strength and inclination angles of earth geomagnetic field. However, at a greater geomagnetic angle, the attenuation rate becomes larger, and the relative phase velocity decreases correspondingly. On the other hand, the influences of the attenuation rates and the phase velocities are weakened by propagating direction. For fundamental modes, there exist directional actions in attenuation rate and phase velocity. For example, the attenuation rate propagating westward will be greater than that propagating eastward, if the relative phase velocity propagating eastward is also smaller than that propagating westward [19].
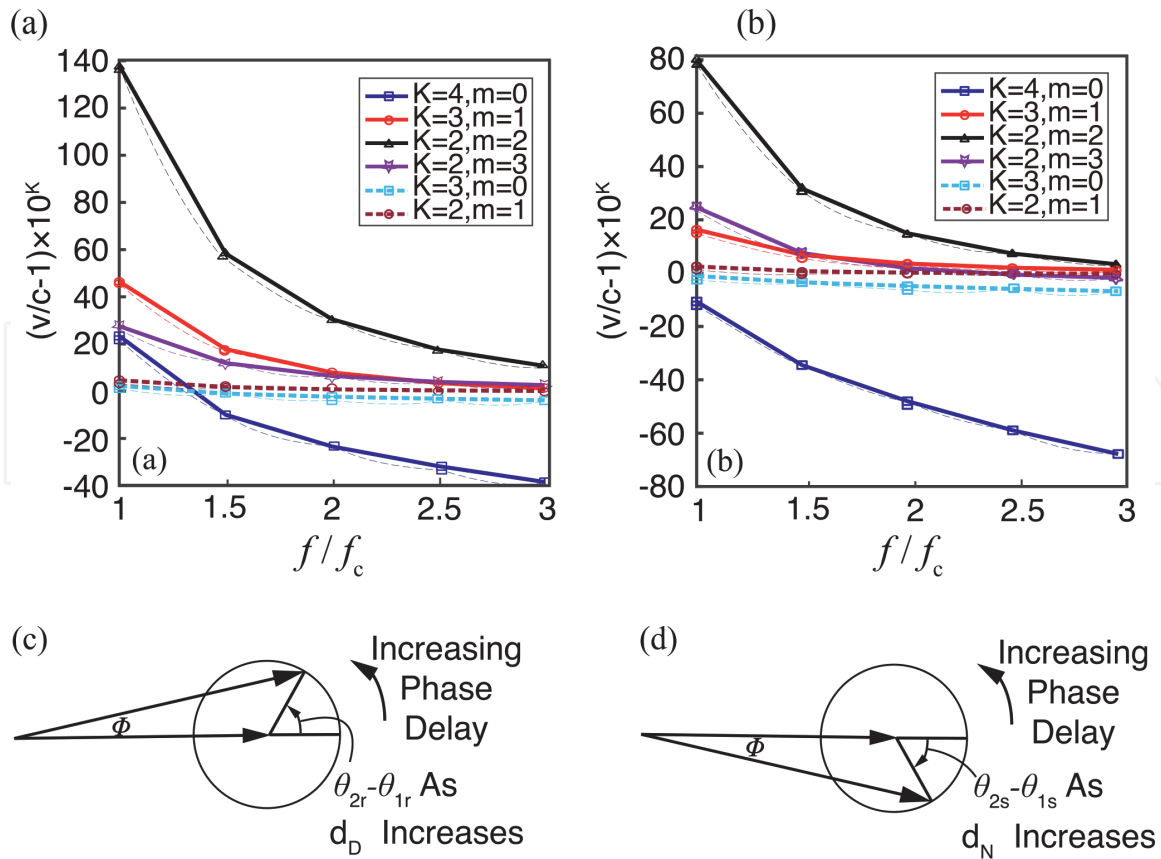
Figure 4.
The relative phase velocity versus the relative frequency f/f_c with (a) $h = 70km$, (b) $h = 90km$, (c) phase delay of d_{D-N}, and (d) phase delay of d_{N-D}. Solid lines (——) are for earth geomagnetic inclination angle of $80°$, and dashed lines (----) are for earth geomagnetic field inclination angle of $90°$.

3. Mode interferences of VLF waves in an anisotropic waveguide due to sunrise and sunset

In this section, the orthogonal properties of basis functions are considered at each side of daytime and nighttime waveguides, respectively, while the ionosphere layer has been treated as anisotropic plasma. The transmission and reflection coefficients are determined by the resulting linear equations from field matching. Thus, the mode-conversion coefficients are obtained for VLF waves propagating in the terrestrial waveguide during sunrise and sunset.

3.1 Mode-conversion coefficients across abrupt discontinuity

The idealized model representing the sunrise or sunset transition is depicted in **Figure 5**, where a cascading anisotropic waveguide is formed by two sections with different effective heights. Each section of the ionosphere layer is regarded as anisotropic plasma, and the waveguide is occupied by the free space, characterized by the permeability μ_0 and the uniform permittivity ε_0. The spherical earth is characterized by μ_0, uniform permittivity of ε_g, and conductivity of σ_g. In **Figure 5**, the effective height of ionosphere $h(x)$ is given by a unit step function, defined by $h(x) = h_A + (h_B - h_A)u(x)$. Thus, at the junction with $x' = 0$, it can be analyzed as a two-port waveguide. In region A, the electromagnetic field can be expressed by the summation of excited wave modes. Let a^A and b^A be vectors in terms of the amplitudes of forward wave and backward wave vectors, respectively, and $\tilde{F}^A$ and $\tilde{G}^A$ be row vectors representing the height-gain functions of TM mode and TE mode, respectively.
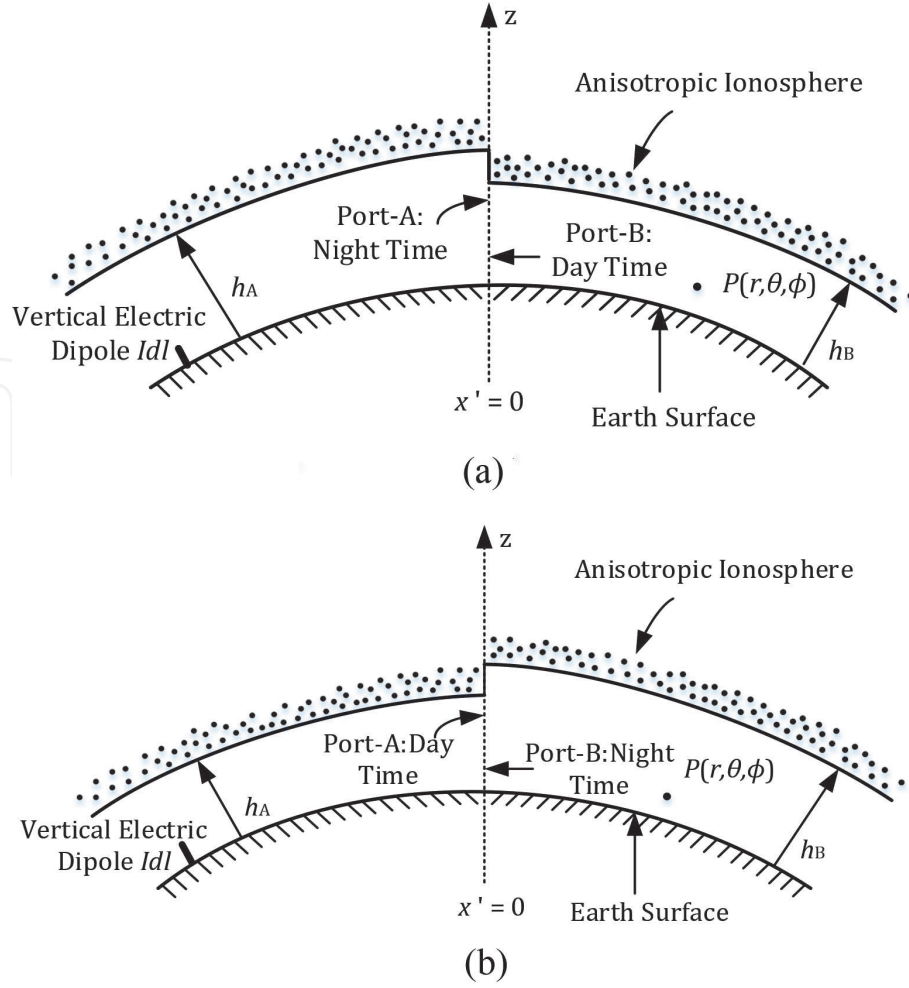
Figure 5.
Geometry of transitional regions in the nonuniform terrestrial waveguides with an abrupt effective height change of 20 km caused by sunset and sunrise, respectively. (a) Night-to-day transition; (b) day-to-night transition.

In region $A(x' > 0)$, the excited wave modes are expressed as follows:

$$
\left.
\begin{aligned}
E_r &= \sum a_n^A F_n^{+A}(z) e^{ik\beta_n^{+A} x'} + \sum b_n^A F_n^{-A}(z) e^{-ik\beta_n^{-A} x'} \\
E_\phi &= \sum a_n^A G_n^{+A}(z) \left[\beta_n^{+A}\right]^{-1} e^{ik\beta_n^{+A} x'} \\
&\quad - \sum b_n^A G_n^{-A}(z) \left[\beta_n^{-A}\right]^{-1} e^{-ik\beta_n^{-A} x'} \\
H_r &= \sum a_n^A G_n^{+A}(z) e^{ik\beta_n^{+A} x'} + \sum b_n^A G_n^{-A}(z) e^{-ik\beta_n^{-A} x'} \\
H_\phi &= - \sum a_n^A F_n^{+A}(z) \left[\beta_n^{+A}\right]^{-1} e^{ik\beta_n^{+A} x'} \\
&\quad + \sum b_n^A F_n^{-A}(z) \left[\beta_n^{-A}\right]^{-1} e^{-ik\beta_n^{-A} x'}
\end{aligned}
\right\}
\tag{16}
$$

In Eq. (16), the different phase velocities, attenuation rates, and height functions are taken into consideration for the incident wave and the reflected wave for each wave type, respectively. In region $B(x' > 0)$, we have

$$
\left.
\begin{aligned}
E_r &= \sum a_n^B F_n^{+B}(y) e^{ik\beta_n^{+B} x'} \\
E_\phi &= \sum a_n^B G_n^{+B}(y) \left[\beta_n^{+B}\right]^{-1} e^{ik\beta_n^{+B} x'} \\
H_r &= \sum a_n^B G_n^{+B}(y) e^{ik\beta_n^{+B} x'} \\
H_\phi &= -\sum a_n^B F_n^{+B}(y) \left[\beta_n^{+B}\right]^{-1} e^{ik\beta_n^{+B} x'}
\end{aligned}
\right\}
\tag{17}
$$

$$
G_n(z) = \Delta_{Emn} g_n(z)
\tag{18}
$$

in which $F_n(z)$ and $G_n(z)$ are the elements of the column vector of height-gain functions.

The superscript B is designated instead of A by different matrix quantities. The element $Y_n(z)$ represents the main element of diagonal matrix for the wave admittance.

At the junctions of day and night sections, the interferences of VLF radio waves occur due to discontinuity of abrupt effective heights. Assume that the electromagnetic waves are incident at the junction from port A in **Figure 1(a)**:

$$
a^B = S^{BA} a^A ; \quad b^A = S^{AA} a^A
\tag{19}
$$

The symbol S^{BA} is determined by a square transmission scattering matrix, whose element S_{nm}^{BA} is the complex amplitude of the nth transmitted mode through the junction at $x' = 0$ from port A. And the symbol S^{AA} is a square reflection scattering matrix, whose element S_{nm}^{AA} is determined by the complex amplitude of the nth reflected mode when the mth mode of unit amplitude is incident at the junction $x' = 0$ from port A. Similarly, the superscripts A and B are interchanged as the above quantities related to wave incidented from port B.

3.1.1 Field matching

At the junction of the waveguide sections with $(x' = 0)$, the boundary condition is applied as follows:

$$
\tilde{F}^{+A} a^A + \tilde{F}^{-A} S^{AA} a^A = \tilde{F}^{+B} S^{BA} a^A
\tag{20}
$$

$$
\tilde{G}^{+A} Y^{+A} a^A - \tilde{G}^{-A} Y^{-A} S^{AA} a^A = \tilde{G}^{+B} Y^{+B} S^{BA} a^A
\tag{21}
$$

$$
\tilde{G}^{+A} a^A + \tilde{G}^{-A} S^{AA} a^A = \tilde{G}^{+B} S^{BA} a^A
\tag{22}
$$

$$
\tilde{F}^{+A} Y^{+A} a^A - \tilde{F}^{-A} Y^{-A} S^{AA} a^A = \tilde{F}^{+B} Y^{+B} S^{BA} a^A
\tag{23}
$$

in which the column vectors Y^A and Y^B stand for the characteristic admittance diagonal matrices for the propagating modes in section A and section B, respectively. The superscript "+" or "−" represents the directed wave or reflected wave at each port, respectively.

3.1.2 VLF waves across abrupt junctions

Taking into account the properties of height-gain functions, the row vectors $\tilde{F}^A$ and $\tilde{G}^A$ at port A are orthogonal over the interval $(0 \leq h \leq h_A)$. Pre-multiply (20) and (22) by the column vectors F^{+B} and $\rho \tilde{G}^B$, and then integrate over the interval $(0, h_A)$, respectively; add up them. Similarly, pre-multiply (21) and (23) by the column vectors F^{+B} and $\rho \tilde{G}^B$, and then integrate over the interval $(0, h_A)$, respectively; add up them. It is noted that the vector a^A can be chosen arbitrarily and ρ is defined by $\rho = \Delta_{12}/\Delta_{21}$; it can be obtained that

$$\left(C^{++B}\ ^A + D^{++B}\ ^A \right) + \left(C^{+-B}\ ^A + D^{+-B}\ ^A \right) S^{AA} = W^B S^{BA} \tag{24}$$

$$W^A Y^{+A} - W^{+-A}\ ^A Y^{-A} S^{AA} = C^{++A}\ ^B Y^{+B} S^{BA} \tag{25}$$

in which matrix $W^{A,B}$ are diagonal matrices because of the orthogonal property of the height functions. Finally, we have

$$S^{BA} = [W^B]^{-1} \left[C^{++B}\ ^A + D^{++B}\ ^A + \left(C^{+-B}\ ^A + D^{+-B}\ ^A \right) S^{AA} \right] \tag{26}$$

$$S^{AA} = \left\{ W^{+-A}\ ^A Y^{-A} + C^{++A}\ ^B Y^{+B} [W^B]^{-1} \left[C^{+-B}\ ^A + D^{+-B}\ ^A \right] \right\}^{-1}$$
$$\times \left\{ W^A Y^{+A} - C^{++A}\ ^B Y^{+B} [W^B]^{-1} \left[C^{++B}\ ^A + D^{++B}\ ^A \right] \right\} \tag{27}$$

It yields

$$E - X \approx [E + X] S^{AA} \tag{28}$$

in which

$$X \approx \left[Y^{-A} \right]^{-1} \left[W^{+-A}\ ^A \right]^{-1} C^{++B}\ ^A Y^{+B} [W^B]^{-1} \left(C^{+-B}\ ^A + D^{+-B}\ ^A \right) \tag{29}$$

Therefore, the reflection scattering matrix can be approximated by

$$S^{AA} = \Delta^{AA} \left(E - \Delta^{AA} \right)^{-1} = \sum_{k=0}^{\infty} \left(\Delta^{AA} \right)^k \tag{30}$$

with

$$\Delta^{AA} = \frac{1}{2}(E - X) \approx \frac{1}{2} \left(E - \left[Y^{-A} \right]^{-1} \left[W^{+-A}\ ^A \right]^{-1} C^{++B}\ ^A Y^{+B} [W^B]^{-1} \left(C^{+-B}\ ^A + D^{+-B}\ ^A \right) \right) \tag{31}$$

where the elements of the matrices $C^{+\pm}_{nm}{}^B$, $D^{+\pm}_{nm}{}^B$, and $W^{A,B}_{nn}$ are obtained by

$$
\overset{+\pm}{C_{nm}^{B}} = \int_{0}^{h_A} \left[F_n^{+B}(y) F_m^{\overset{\pm}{A}}(y) + \rho G_n^{+B}(y) G_m^{\overset{\pm}{A}}(y) \right] dy \; \overset{+\pm}{C_{mn}^{A}}
$$

$$
\int_{0}^{h_A} \left[F_m^{+A}(y) F_n^{\overset{\pm}{B}}(y) + \rho G_m^{+A}(y) G_n^{\overset{\pm}{B}}(y) \right] dy
\tag{32}
$$

and

$$
\overset{+\pm}{D_{nm}^{B}} = \int_{h_A}^{h_B} \left[F_n^{+B}(y) F_m^{\overset{\pm}{A}}(y) + \rho G_n^{+B}(y) G_m^{\overset{\pm}{A}}(y) \right] dh
$$

$$
\approx \left[F_n^{+B}(y) F_m^{\overset{\pm}{A}}(y) + \rho G_n^{+B}(y) G_m^{\overset{\pm}{A}}(y) \right]_{h_A} (h_B - h_A)
$$

$$
+\frac{(h_B - h_A)^2}{2} \left[F_n^{+B}{}'(y) F_m^{\overset{\pm}{A}}(y) + \rho G_n^{+B}(y)' G_m^{\overset{\pm}{A}}(y) \right.
$$

$$
\left. + F_n^{+B}(y) F_m^{\overset{\pm}{A}}{}'(y) + \rho G_n^{+B}(y) G_m^{\overset{\pm}{A}}{}'(y) \right]_{h_A}
\tag{33}
$$

where

$$
W_{nn}^{A} = \int_{0}^{h_A} \left[\left(F_n^{+A}(y) \right)^2 + \rho^{+A} \left(G_n^{+A}(y) \right)^2 \right] dy
\tag{34}
$$

$$
W_{nn}^{B} = \int_{0}^{h_B} \left[\left(F_n^{+B}(y) \right)^2 + \rho^{+B} \left(G_n^{+B}(y) \right)^2 \right] dy
\tag{35}
$$

in which $F_n^{+B}(y)$ and $G_n^{+B}(y)$ are defined by Eq. (4) to Eq. (5), respectively. It is noted that for the case where the ionosphere may be considered as isotropic, the resulted coefficients can be reduced to the early analysis [13]. It is known from Eq. (23) that the reflection scattering matrix can be approximated in the form of

$$
\Delta^{AA} \approx \sum_{p=0}^{\infty} \left(\frac{1}{2} (E - X) \right)^k
\tag{36}
$$

whose elements are

$$
S_{nm}^{AA} \approx \Delta_{nm}^{AA} = \frac{1}{2} \left(\delta_{nm} - \sum_k \frac{\beta_k^B C_{np}^{++B} {}^{A} \left(C_{pm}^{+-B} {}^{A} + D_{pm}^{+-B} {}^{A} \right)}{\beta_k^A W_{nn}^A W_{kk}^B} \right)
\tag{37}
$$

in which the delta function δ_{nm} is defined by an impulsive-like function with $\delta_{nn} = 1 (n = 1)$. Correspondingly, the element of transmission scattering matrix can be obtained as follows:

$$S_{nm}^{BA} \approx \frac{C_{nm}^{++A\;B}}{W_{nn}^{B}} + \sum_{k=0}^{\infty} \frac{\left(C_{nk}^{+-A\;B} + D_{nk}^{+-A\;B}\right)}{W_{nn}^{B}} S_{km}^{AA} \tag{38}$$

It is noted that Eq. (37) and Eq. (38) define the reflection matrix S^{AA} and scattering matrix S^{BA} are analogous to the definitions in the transmission line theory, suppressed by the normalized load admittance.

3.2 VLF waves across cascaded waveguides

Due to the revolution of the earth, the boundary of daytime and nighttime regions is moving over time. Thus, in the period of the daytime and nighttime transitions, the received phase of VLF radio waves in a receiving antenna appears a regular fluctuation. This is called the transition period interfered by mode conversions.

In **Figure 6**, the geometries of the transition model are presented by cascaded terrestrial waveguides, respectively. These models are approximated by an inhomogeneous waveguide represented in **Figure 7** with a varying height. The height function can be defined as follows:

$$h(x) = \frac{1}{2}(h_N + h_D) + \Delta h \cdot cos\left(\frac{\pi u}{L}\right) \tag{39}$$

in which

$$u(x) = \left(1 - 2\frac{\alpha}{\pi}\right)x + L \cdot \frac{\alpha}{\pi} + \left(2\frac{\alpha}{\pi} - 1\right)x_N \tag{40}$$
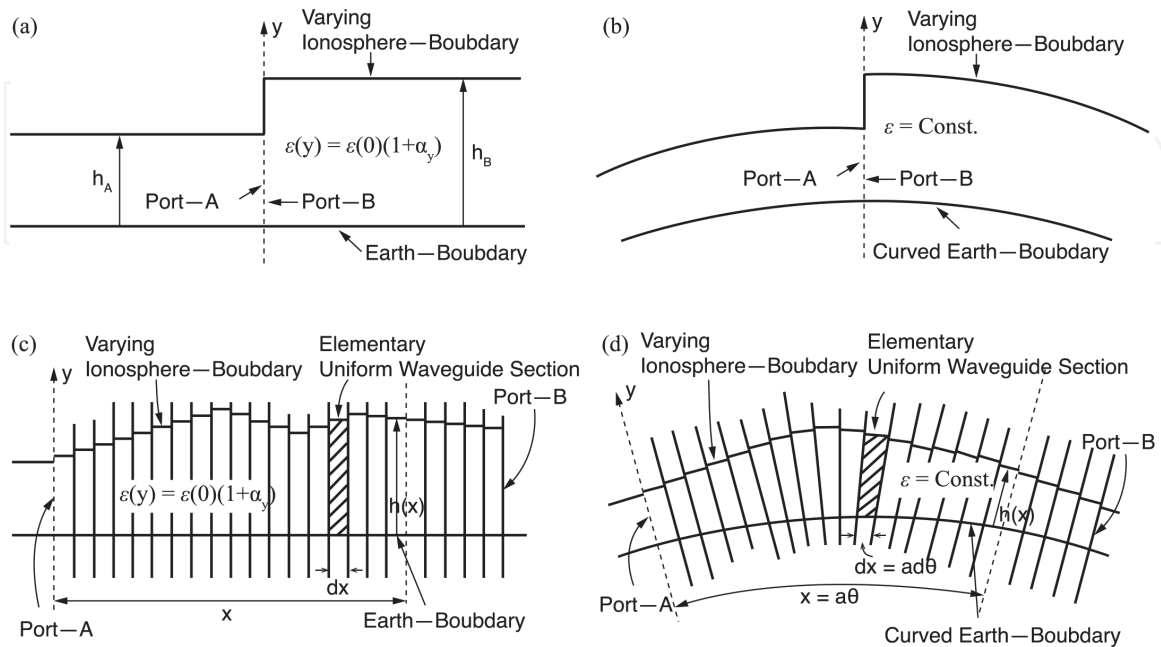
with $x = x_N + \Delta x$.

Figure 6.
Varying height profile in the transition region between the night and day paths with (a) planar model in abrupt discontinuity; (b) spherical model in discontinuity; (c) cascaded planar model in abrupt discontinuity; and (d) cascaded spherical model in discontinuity.
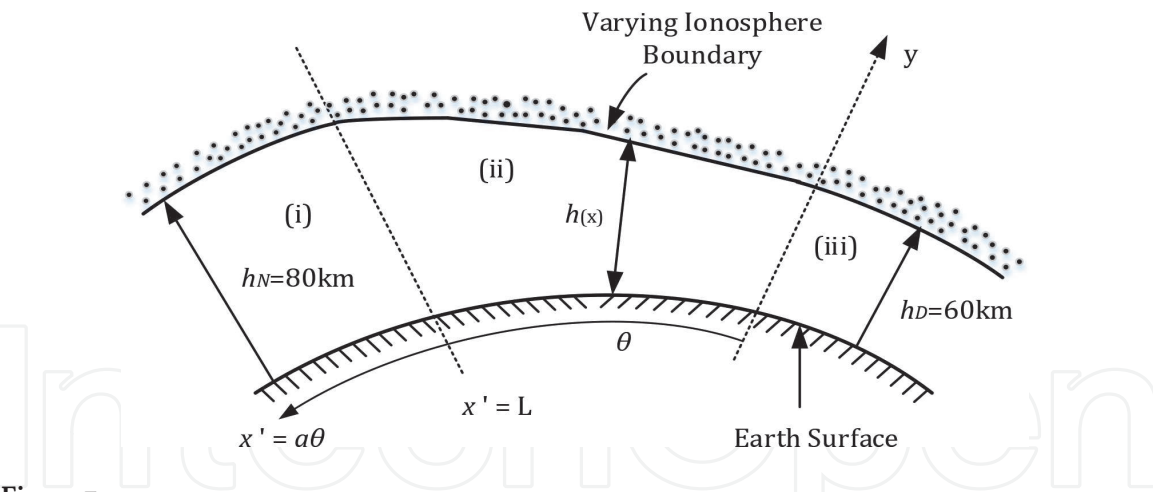
Figure 7.
Gradually varying height profile in the transition region between the night and day paths with (i) nighttime section, (ii) transition section with varying ionospheric effective height, and (iii) daytime section.

In this case, the scattered coefficients derived in Eq. (36) to Eq. (37) can be developed as follows:

$$S_{nm}^{BA} = \left[C_{nm}^{++BA} + D_{nm}^{++BA} + \left(C_{nm}^{+-BA} + D_{nm}^{+-BA} \right) S_{nm}^{AA} \right] / W_{nn}^{B} \tag{41}$$

So that, we have

$$\frac{dS_{nm}^{BA}}{dx} = \left. \frac{S_{nm}^{BA}}{dh} \frac{dh}{dx} \right|_{h_A = h_B = h(x)}$$

$$- \left[\frac{dC_{nm}^{++BA}}{dh} + \frac{dD_{nm}^{++BA}}{dh} + \frac{d\Delta_{nm}^{AA}}{dh} \right] \left. \frac{dh}{dx} \right|_{h_A = h_B = h(x)} \tag{42}$$

and

$$\frac{S_{nm}^{AA}}{dx} = \left. \frac{S_{nm}^{AA}}{dh} \frac{dh}{dx} \right|_{h_A = h_B = h(x)}$$

$$\left. \frac{d\Delta_{nm}^{AA}}{dh} \frac{dh}{dx} \right|_{h_A = h_B = h(x)} \tag{43}$$

in which

$$\left. \frac{d\Delta_{nm}^{AA}}{dh} \right|_{h(x)} \frac{dh}{dx} = \frac{S_{nm}^{AA}}{dx}$$

$$- \left[\frac{dC^{++BA}}{dh} + \frac{1}{2} \frac{dD^{++BA}}{dh} \right] \left. \frac{dh}{dx} \right|_{h_A = h_B = h(x)} \tag{44}$$

and

$$\frac{dS_{nm}^{BA}}{dx} = \frac{\Delta h}{2} \frac{dD^{++BA}}{dh} \left(2\frac{\alpha}{\pi} - 1 \right) \sin\left(\frac{\pi y}{L} \right) \tag{45}$$

$$\frac{dh}{dx} = \Delta h \cdot sin\left(\frac{\pi y}{L}\right)\left(2\frac{\alpha}{\pi} - 1\right) \tag{46}$$

respectively.

3.3 Computation and discussion

In the following computations, numerical solutions are obtained by computer software, such as Matlab, to quantitatively evaluate the resulted formulas for mode-conversion coefficients of VLF radio waves due to sunrise and sunset.

3.3.1 Mode-conversion coefficients of reflected and scattered vectors

During long-distance propagation across the transition regions, several modes contribute to the net fields. Based on the derived formulas, the vertical electric field component can be determined by the distance variations, so that the mode-conversion coefficients can be obtained, correspondingly. Consider that the altitude of the lower ionosphere is assumed to be at **90km** and **70km** for nighttime and daytime, respectively, and the radius of earth is taken by $a = 6370km$. In the computations, the ground can be characterized by the plane sea surface with conductivity and relative dielectric constant of it being $\sigma_g = 4$ S/m and $\varepsilon_{rg} = 80$, respectively. When both receiving antenna and radiating antenna are located on the ground surface, the resulted mode-conversion coefficients are computed and summarized in **Tables 1** and **2** for distinct operating frequencies at $f = 10kHz$ and at

Nth	Anisotropic ionosphere			
	Re (S_{1m}^{BA})	Im (S_{1m}^{BA})	Re (S_{1m}^{AA})	Im (S_{1m}^{AA})
1	1.0554	0.1188i	−1.5452	−0.0717i
2	−0.5785	−0.0165i	0.4090	0.0143i
3	0.2533	0.0071i	−0.1753	−0.0061i
4	−0.1415	−0.0039i	0.0974	0.0034i
5	0.0902	0.0025i	−0.0620	−0.0022i

Table 1.
The transmitted coefficients and scattered coefficients S_{1m}^{BA} and S_{1m}^{AA}, at f = 10 kHz.

Nth	Anisotropic ionosphere			
	Re (S_{1m}^{BA})	Im (S_{1m}^{BA})	Re (S_{1m}^{AA})	Im (S_{1m}^{AA})
1	0.9883	0.0014i	−0.0939	−0.0372i
2	0.0946	0.0080i	0.1188	0.0074i
3	−0.0167	−0.0038i	−0.0509	−0.0032i
4	0.0069	0.0021i	0.0283	0.0018i
5	−0.0038	−0.0014i	−0.0180	−0.0011i
6	0.0025	0.0009i	0.0125	0.0008i
7	−0.0017	−0.0007i	−0.0091	−0.0006i
8	0.0013	0.0005i	0.0070	0.0004

Table 2.
The transmitted coefficients and scattered coefficients S_{1m}^{BA} and S_{1m}^{AA}, at f= 20 kHz.

$f = 20kH$, respectively. The computation is obtained by choosing a nighttime-to-daytime propagation path with an abrupt effective height change of ionosphere by $20km$ across the discontinuity.

Technically, the magnitudes of the first-second and second-first mode-conversion coefficients will affect more than the higher modes [19]. It is seen that more summation terms would be required to guarantee accuracies of calculations at high operating frequencies. In **Tables 1** and **2**, the determined elements of the reflected and transmitted scattering matrix are calculated by Eq. (36) and Eq. (37), respectively. The derived matrix is subjected to modal equations by Eq. (8). It is noted that for more complicated case of varying ionosphere heights, these coefficients can be derived by Eq. (42) and Eq. (43) which are not addressed in the illustrative example for simplicity.

3.3.2 Interference behaviors of VLF radio waves across abrupt discontinuity

For a better understanding of the interference pattern by the use of the obtained formulas, the following computations are developed when the ionosphere layer is composed of a succession of two bounded layers, each with a distinct character. Assuming that the transmitting antenna is placed on the sea surface in region *A*, the magnitudes of components for VLF radio waves vary as functions of the propagation distances and observation heights, which is plotted in **Figure 8**. It is noted that the altitude *h* enters in the calculation of excitation factors and of field amplitudes; and *h* of the waveguide region around the source (section *A* in **Figure 5**) is left the same as in the original mode calculations [**Figure 8(a)** for nighttime $h_N = 90km$ and **Figure 8(b)** for daytime $h_D = 70km$, where the subscripts *N* and *D* refer to nighttime and daytime conditions, respectively]. The other waveguide region of the discontinuity problem does not contain a source [section *B* of **Figure 5(a)** and **Figure 5(b)**]; after determining the attenuation rates and phase velocities (or the transmitting scattering coefficients S_{nm}^{DN}) for the waveguide modes of this source-free region with the calculated equivalent ionospheric surface impedance matrix to be discussed in the next section, the scattered fields in the waveguide in both sections due to sunrise can be calculated at any arbitrary altitude.

From **Figure 8(c)** and **Figure 8(d)**, the distributions of the electromagnetic field strength for VLF waves due to sunrise are depicted at the operating frequency *f* = 10 kHz. From **Figure 8(e)** to **Figure 8(g)**, it is depicted that the field components in the sections are quite different at different propagation distances and different altitudes. Obviously, the interference occurs at the abrupt junction of two cascaded waveguides.

In a similar manner, the wave components are evaluated through a D-to-N propagation path. Considering that all parameters are chosen as same as those in **Figure 8**, the spatial distribution of the scattered field is depicted in **Figure 9(d)** through a D-to-N propagation path. However, it is seen that the interference pattern is unlikely in agreement with reciprocity in which the section on the right side is subjected to different incident angles. This shall also be affected by the earth geomagnetic field inclination angle and the propagation angle. However, the proposed computational scheme is in advantage of providing a straightforward in calculation for nonreciprocal model. In **Figure 9(e)**, the electromagnetic field in the transition region by corresponding formulas is plotted versus the propagation distance in the same figure at the operating frequency $f = 10kHz$, in daytime and nighttime, respectively. The interference mechanism by D-to-N propagation path is similar to that of N-to-D propagation path in **Figure 10(a)**, and the field strength is coherent near the junction.
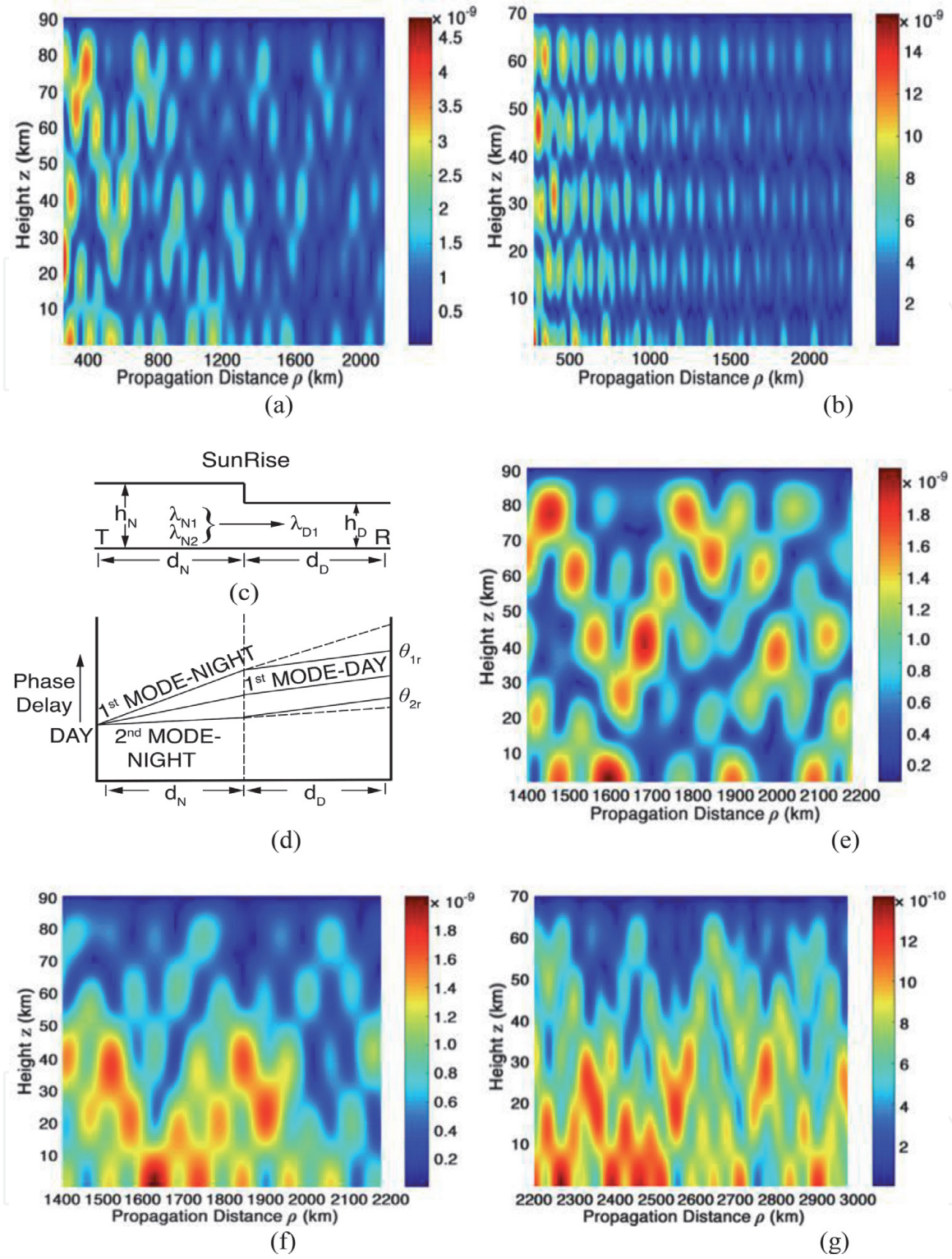
Figure 8.
Illustrative example of mode interferences in N-to-D propagation path with spatial distributions of the field component E_r *in* V/m, *at the operating frequency* f = 10 kHz; *with parameters taken by* $\varepsilon_g = 80$, $\sigma_g = 4$ S/m, $h_N = 90km$, *and* $h_D = 70km$; *with (a) incident field in nighttime, (b) incident field in daytime, (c) geometry of waveguide, (d) mode interference model, (e) incident field in region a, (f) scattered field in region a, and (g) transmitted field in region B.*

3.3.3 Comparing with the experimental data for the VLF radio wave at 20.5 kHz due to sunrise

In **Figure 10(a)**, the interfered electric field due to sunrise is computed as comparing with that for a homogeneous waveguide representing for daytime and nighttime, respectively. It is seen that the interference subjected to mode
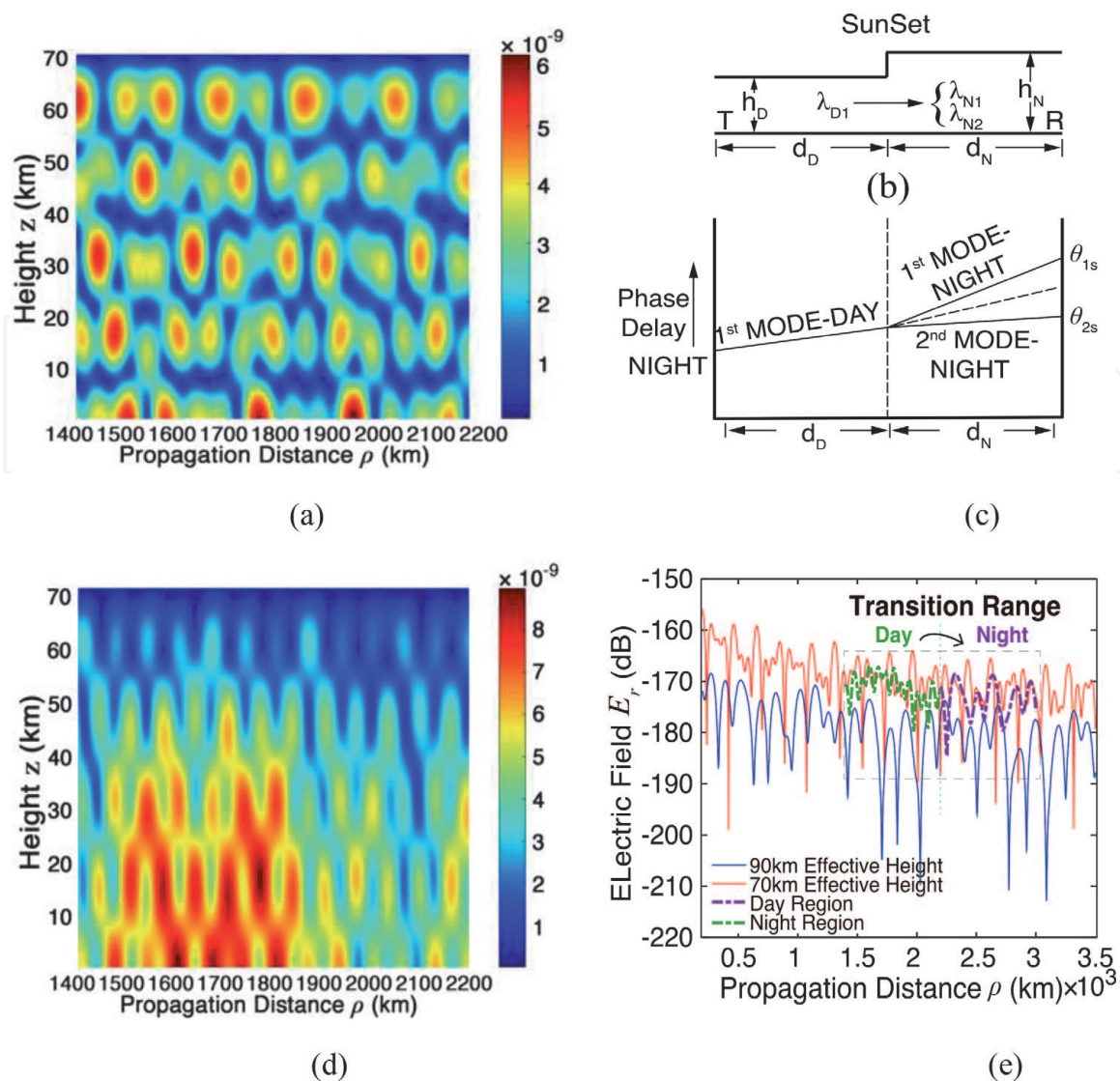
Figure 9.
Illustrative example of mode interferences in D-to-N propagation path with spatial distributions of the field component E_r in V/m, at the operating frequency $f = 10$ kHz; $\varepsilon_g = 80$, $\sigma_g = 4$ S/m, $h_N = 90km$, and $h_D = 70km$, with (a) incident wave in region a, (b) geometry of waveguide, (c) mode interference model, (d) scattered wave in region a, and (e) the magnitudes of the field component E_r in dB versus the propagation distance due to sunset.

conversion is resulted from discontinuousness from distinct ionosphere boundaries due to day and night propagation paths.

In order to validate of the proposed computational scheme, the simulation has been compared with the experimental data addressed in a recent paper [25] in **Figure 10(b)**. The radiation power is 250 kw, and the radiating device is chosen by un-directional antenna. The experimental data are measured at the operating frequency $f = 20.5$ kHz in the same location from the time 4 o'clock a.m. to 8 o'clock a.m. in east-to-west direction. Taking into account that both the observation point and transmitting antennas are located on the ground, with the same operating frequency, the conductivity and relative dielectric constant of sea water being $\sigma_1 = 4$ S/m and $\varepsilon_{r1} = 80$, the amplitudes of synthetic fields are computed along an idealized N-to-D transition propagation path. The synthetic fields contain two parts: the first section before a sunrise line (including the incident wave and scattered wave) and the second section across a sunrise line (standing for the transmitted wave).

It is shown from **Figure 10(b)** that the calculated result as synthetic field being interfered by multimode-conversion effect is closer to the experimental data measured on 4 o'clock and 5 o'clock than measured on 6, 7, and 8 o'clock data near the
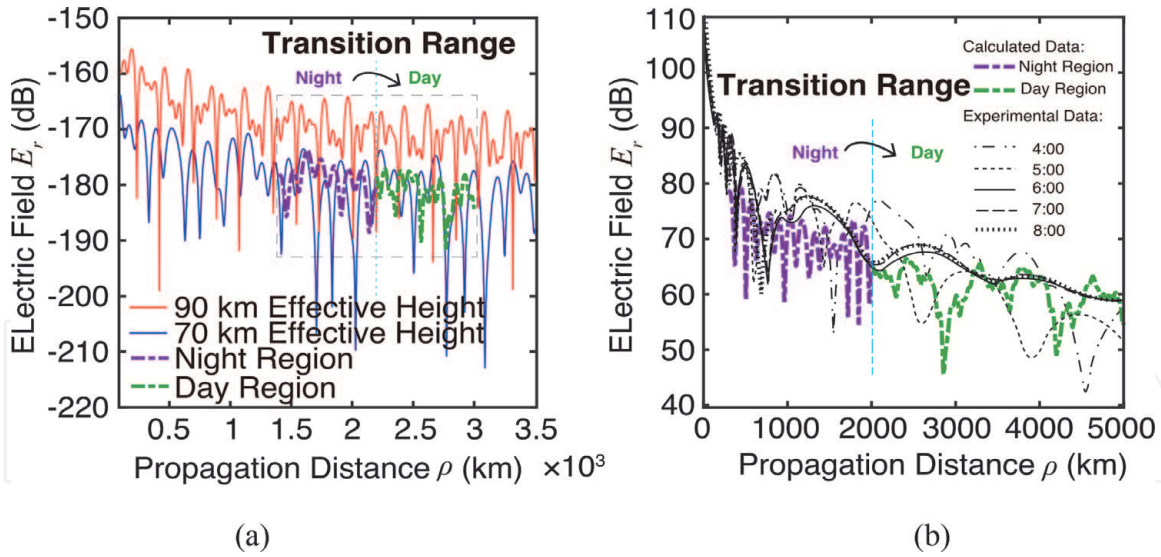
Figure 10.
The magnitudes of the field component E_r in dB versus the propagation distance due to sunrise in nighttime, daytime, and transition range, respectively, at the operating frequency f = 10 kHz; $\varepsilon_g = 80$, $\sigma_g = 4$ S/m, $h_N = 90km$, and $h_D = 70km$, with (a) the simulated results comparing the transition path in N-to-D with daytime and nighttime propagations and (b) the calculated result comparing with experimental data, respectively.

sunrise line. Additionally, the measured data after 6 o'clock does not change too much since process of sunrise passed. Taking into account that the difference between calculated data and the measured data is resulted from the applied models and specific measuring conditions, such as the time, locations, and propagation paths, the proposed computational scheme would be more helpful by adjusting it into more practical models than a simple structure with abrupt discontinuity in height boundaries.

4. Conclusions

In this chapter, the effect of multimode interferences is investigated for VLF radio waves due to sunrise and sunset based on an idealized cascaded anisotropic inhomogeneous terrestrial waveguide. The coefficients of mode conversion for scattered vectors and transmitted vectors are evaluated at the junction of abrupt discontinuity representing the nighttime and daytime transition. The treatment provided can be enhanced in the future by a more practical terrestrial waveguide with varying effective ionosphere height rather than the abrupt one. The study may provide with some help in the applications of long-distance communication and navigation.

Acknowledgements

Conflict of interest

No potential conflict of interest was reported by the authors.

Author details

Ting Ting Gu[1] and Hong Lei Xu[2]*

1 Department of Information Science and Electric Engineering, Zhejiang University, Hangzhou, China

2 Science and Technology on Electromagnetic Scattering Laboratory, Beijing, China

*Address all correspondence to: xhl_207@126.com

IntechOpen

References

[1] Martin HG. Wave-guide mode propagation of very low frequency radio waves. Journal of Atmospheric and Terrestrial Physics. 1961;**20**:206-209. DOI: 10.1016/0021-9169(61)90078-2

[2] Rieker J. Sunset and sunrise in the ionosphere: Effects on the propagation of longwaves. Journal of Research of the National Bureau of Standards. 1963;**67D**:119. DOI: 10.6028/jres.067D.016

[3] Crombie DD. Periodic fading of VLF signals received over long paths during sunrise and sunset. Journal of Research of the National Bureau of Standards. 1964;**68D**:27-34. DOI: 10.6028/jres.068D.012

[4] Ries G. Results concerning the sunrise effect of VLF signals propagated over long paths. Radio Science. 1967;**2**:531-538. DOI: 10.1002/rds196726531

[5] Smith R. Mode conversion coefficients in the earth-ionosphere waveguide for VLF propagation below a horizontally stratified, anisotropic ionosphere. Journal of Atmospheric and Terrestrial Physics. 1977;**39**:539-543. DOI: 10.1016/0021-9169(77)90163-5

[6] Devi MI, Khan I, Madhusudhana RDN. A study of VLF wave propagation characteristics in the earth-ionosphere waveguide. Earth, Planets and Space. 2008;**60**:737-741

[7] Steele FK, Crombie DD. Frequency dependence of VLF fading at sunrise. Radio Science. 2015;**2**:547-549. DOI: 10.1002/rds196726547

[8] Walter F, Scarabucci RR. VLF propagation in the magnetosphere during sunrise and sunset hours. Radio Science. 1975;**10**:965-971. DOI: 10.1029/rs010i011p00965

[9] Rodger CJ, Brundell JB, Dowden RL, Thomson NR. Location accuracy of long distance VLF lightning location network. Annales Geophysicae. 2004;**22**:747-758. DOI: 10.5194/angeo-22-747-2004

[10] Bennett AJ, Gaffard C, Nash J, et al. The effect of modal interference on VLF long-range lightning location networks using the waveform correlation technique. Journal of Atmospheric and Oceanic Technology. 2011;**28**:993-1006. DOI: 10.1175/2011JTECHA1527.1

[11] Wait JR. Reflection of VLF radio waves at a junction in the earth-ionosphere waveguide. IEEE Transactions on Electromagnetic Compatibility. 1922;**34**:4-8. DOI: 10.1109/15.121660

[12] Wait JR. Mode conversion and refraction effects in the earth-ionosphere waveguide for VLF radio waves. Journal of Geophysical Research. 1968;**73**:3537-3548. DOI: 10.1029/ja073i017p05809-01

[13] Bahar E. Analysis of mode conversion in waveguide transition sections with surface impedance boundaries applied to VLF radio propagation. IEEE Transactions on Antennas and Propagation. 1968;**16**:673-678. DOI: 10.1109/TAP.1968.1139274

[14] Bahar E. Propagation of radio waves in a model nonuniform terrestrial waveguide. Proceedings of the Institution of Electrical Engineers. 1966;**113**:1741-1750. DOI: 10.1049/piee.1966.0299

[15] Bahar E. Scattering of VLF radio waves in the curved earth-ionosphere waveguide. Radio Science. 1968;**3**:145-154. DOI: 10.1002/rds196832145

[16] Bahar E. Propagation of VLF radio waves in a model earth-ionosphere waveguide of arbitrary height and finite surface impedance boundary: Theory

and experiment. Radio Science. 1966;**1**: 925-938. DOI: 10.1109/ APS.1965.1150285

[17] Galejs J. Propagation of VLF waves below a curved and stratified anisotropic ionosphere. Journal of Geophysical Research. 1964;**69**:3639-3650. DOI: 10.1029 /jz069i017p03639

[18] Galejs J. VLF propagation across discontinuous daytime-to-nighttime transitions in anisotropic terrestrial waveguide. IEEE Transactions on Antennas and Propagation. 1971;**19**: 756-762. DOI: 10.1109/TAP.1971. 1140034

[19] Pan WY, Li K. Excitation and propagation of SLF/ELF electromagnetic waves in the earth-ionosphere waveguide/cavity. In: Pan WY, Li K, editors. Propagation of SLF/ELF Electromagnetic Waves. 1st ed. Hangzhou, CN: Zhejiang University Press; Berlin Heidelberg, GER: Springer-Verlag; 2014. pp. 17-63

[20] Li K. Electromagnetic Fields in Stratified Media. Hangzhou, CN: Zhejiang University Press; Berlin Heidelberg, GER: Springer-Verlag; 2009

[21] Li GZ, Gu TT, Li K. SLF/ELF electromagnetic field of a horizontal dipole in the presence of an anisotropic earth-ionosphere cavity. Applied computational electromagnetics. Society. 2014;**29**:1102-1111

[22] Li K, Sun XY, Zhai HT. Propagation of ELF electromagnetic waves in the lower ionosphere. IEEE Transactions on Antennas and Propagation. 2011;**59**: 661-666. DOI: 10.1109/TAP.2010. 2096391

[23] Wait JR. Electromagnetic Waves in Stratified Media. 2nd ed. New York: Pergamon Press; 1970

[24] Gu TT, Xu HL, Li K. Mode interferences of VLF waves in an anisotropic waveguide due to sunrise and sunset. IEEE Transactions on Antennas and Propagation. 2018:1-1. DOI: 10.1109/TAP.2018.2870347

[25] Wei L, Jiang YZ, Li KF. VLF field strength calculation methods based on waveguide mode. Ship Electronic Engineering. 2011;**59**:661-666